Ag- and Cu-promoted mesoporous Ta-SiO$_2$ catalysts prepared by non-hydrolytic sol-gel for the conversion of ethanol to butadiene

Denis D. Dochain, Ales Styskalik, Damien P. Debecker*

Institue of Condensed Matter and Nanosciences – Université catholique de Louvain. Place Louis Pasteur, 1, 1348 Louvain-la-Neuve, Belgium. *Correspondance: damien.debecker@uclouvain.be

Abstract: The direct catalytic conversion of bioethanol to butadiene, also known as the Lebedev process, is one of the most promising solution to replace the petro-based production of this important bulk chemical. Considering the intricate reaction mechanism – where a combination of acid-catalyzed dehydration reactions and metal-catalyzed dehydrogenation have to take place simultaneously – tailor-made bifunctional catalysts are required. We propose to use non-hydrolytic sol-gel (NHSG) chemistry to prepare mesoporous Ta-SiO$_2$ materials which are further promoted by Ag via impregnation. An acetamide elimination route is presented, starting from silicon teraacetate and pentakis(dimethylamido)tantalum(V), in the presence of a pluronic surfactant. The catalysts display advantageous texture, with specific surface area in the 600-1000 m^2.g^{-1} range, large pore volume (0.6-.1.0 cm^3.g^{-1}), an average pore diameter of 4 nm and only a small contribution from micropores. Using an array of characterization techniques, we show that NHSG allows achieved a high degree of dispersion of tantalum, mainly incorporation as single sites in the silica matrix. The presence of these monomeric TaO$_x$ active sites is responsible for the much higher dehydration ability, as compared to the corresponding catalyst prepared by impregnation of Ta onto a pristine silica support. We attempt to optimize the butadiene yield by changing the relative proportion of Ta and Ag and by tuning the space velocity. We also demonstrate that Ag or Cu can be introduced directly in one step, during the NHSG process. Copper doping is shown to be much more efficient than silver to guide the reaction towards the production of butadiene.
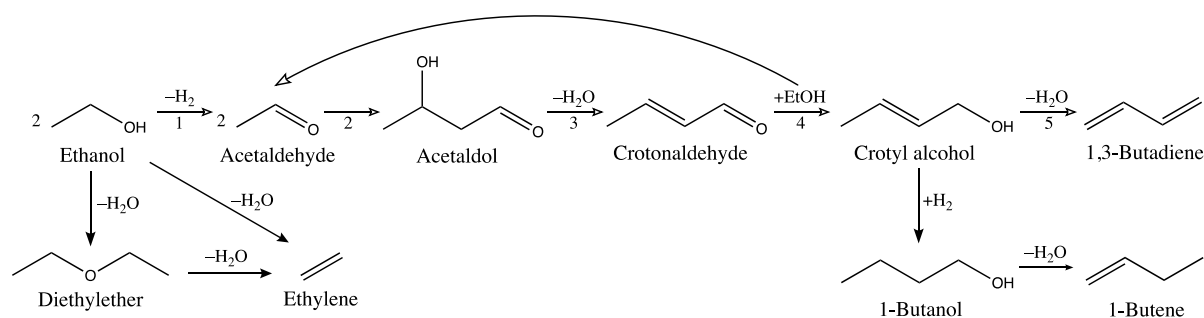
Keywords: Mesoporous metallosilicate, tantalum oxide, bioethanol, bifunctional catalysts, dehydration, dehydrogenation

1. Introduction

1,3-butadiene (BD) is one of the main monomers used in polymer production, mainly for styrene-butadiene rubber and polybutadiene.[1-2] Industrially, the steam cracking of naphta represents a vast majority (ca. 95%) of the butadiene production, as a by-product of ethylene manufacturing.[1-4] The global production of butadiene is rising steadily and sat at around 12000 kT in 2015.[1] Currently, however, butadiene supply tends to decrease with the advent of lighter feedstocks exploitation like shale gas.[1] It should also be mentioned that steam cracking is responsible for 8 % of the global energy consumption and for the release of 180-200 million tons of CO_2 worldwide.[1, 5] Thus, there is a striking tension on the butadiene market and an urgent need for a more sustainable alternative for the production of butadiene.

Bio-based processes as alternatives to petroleum-based production processes are under intense research in the last years.[1, 6-9] A wide range of raw biomass streams can be upgraded, for example by biotechnological processes towards bioethanol. The global production of bioethanol reached 120 billion liter in 2017 and is expected to reach 130 billion liter by 2024.[1] Being recognized as a major platform chemical for the future bio-based chemical industry,[10] bioethanol has a broad scope of applications.[6-7] In particular, the catalytic conversion of ethanol to butadiene is currently attracting great attention.[1-3, 11-13]

While it is long known that butadiene can be obtained from ethanol,[14-15] an intense research effort is currently being paid to understand the working behavior of bifunctional catalysts being able to catalyze this reaction. In fact, two processes are known to convert ethanol into butadiene: the Lebedev process (i.e. the direct conversion of ethanol to butadiene with one catalyst in one reactor), and the Ostromislensky process (i.e. the conversion of a mixture ethanol/acetaldehyde to butadiene, where acetaldehyde is produced in a separate step; two distinct reactors with two different catalyst).[1, 3, 16-17] The Lebedev process is considered more attractive on an environmental and economic point of view.[1] The so called "Kagan mechanism" is generally reported as the most likely reaction pathway for the ethanol to butadiene (ETB) reaction when considering acidic catalysts.[3, 17-18] Scheme 1 shows the complete pathway to obtain butadiene directly from ethanol: the reaction involves an intricate network of dehydrogenation, hydrogen transfer and dehydration steps.[17] This complex mechanism shows the importance of having a multifunctional catalyst possessing correctly balanced redox and acid/base properties to reach high butadiene yield, so as to restrain the formation of by-products such as ethylene, diethylether and unconverted acetaldehyde.[18] In practice, bi-functional catalysts featuring acid sites for dehydration and metallic nanoparticles for dehydrogenation are needed to complete the direct conversion of ethanol to butadiene.
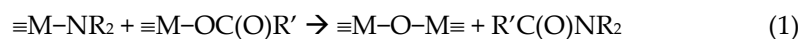

Scheme 1. Kagan mechanism for the direct conversion of ethanol to butadiene in the Lebedev process[17]: (1) non-oxidative dehydrogenation of ethanol (EtOH) to acetaldehyde (AA); (2) condensation of two AA molecules into 3-hydroxybutanal (acetaldol); (3) acetaldol dehydration to crotonaldehyde; (4) production of crotyl alcohol and AA after a Meerwein-Ponndorf-Verley (MPV) reduction involving ethanol; (5) dehydration of crotyl alcohol to butadiene.[17]

The literature describes supported catalysts such as ZrO_2/SiO_2 or Ta_2O_5/SiO_2 promoted with metals like Ag, Co, Cu, Fe or Zn as typical formulations for the Lebedev process.[3, 13, 15, 19-21] In most cases, wet impregnation is used to incorporate the active elements onto a preformed support (e.g.

75　silica). However, such preparation methods show some limitations, especially in terms of control on
76　the speciation of the metal oxide and on the dispersion of metal nanoparticles.[13, 19] Therefore, more
77　advanced preparation techniques have also been proposed, in a search for improved performance.
78　Recently, for example, Ta-based zeolites (Ta-SiBEA) promoted with Ag, Cu or Zn were reported to
79　display high butadiene selectivity, owing to the presence of isolated Ta(V) species which give acidic
80　properties to the catalyst.[16, 22] This shows the importance of controlling the type of active sites during
81　the synthesis process to obtain the required acidity.
82　　　Sol-gel processes have emerged as promising routes for the preparation of advanced
83　heterogeneous catalysts.[23-24] In classical sol-gel methods, molecular precursors undergo hydrolysis
84　and inorganic polycondensation reactions to form, in a bottom-up fashion, a solid material with the
85　desired properties. Importantly, wide ranges of composition can be envisaged, and the texture of the
86　solid can be fine-tuned, for example by using appropriate sacrificial templating agents. Nevertheless,
87　classical – hydrolytic – sol-gel chemistry routes face two limitations: (i) markedly different reactivity
88　of different precursors often leads to inhomogeneous solids and (ii) water elimination during drying
89　tends to cause pore collapse due to high surface tension. One possible solution to avoid these issues
90　is to work in non-aqueous conditions where oxo bridges are formed with the help of oxygen donors
91　other than water.[25-30] In these "non-hydrolytic sol-gel" (NHSG) routes, the reactivity of different
92　precursors tends to be levelled off, leading to highly homogeneous metallosilicate materials. Also,
93　working in organic solvents with low surface tension prevents the pores collapse during drying
94　which leads to highly porous materials.[25, 28] NHSG routes were reported to lead to various types of
95　metallosilicate catalysts showing high performance in many different fields of applications, including
96　olefin metathesis,[31-32] olefin epoxidation,[33-34] mild oxidation of sulphur compounds,[35] aminolysis,[27]
97　photocatalysed aniline degradation,[36] etc. To the best of our knowledge, Ta oxide-based materials
98　prepared by NHSG have never been reported in the literature.
99　　　In this work, we use the non-hydrolytic acetamide elimination route (Eq. 1)[28] to obtain highly
100　homogeneous and mesoporous Ta-silicate materials. The incorporation of tantalum into the silica
101　matrix is described using X-ray photoelectron spectroscopy (XPS), infrared and diffuse reflectance
102　UV spectroscopies. We use NH_3-TPD to quantify the acid sites in the catalysts. The new catalysts are
103　systematically compared to a catalyst that was prepared by simple wet impregnation of tantalum
104　ethoxide on a silica support also prepared by NHSG. Ta-based materials were impregnated with
105　silver in order to obtain a bifunctional catalyst exhibiting also redox properties. The catalysts are
106　tested in the ethanol to 1,3-butadiene reaction. Several effects influencing butadiene yield are
107　discussed: (i) the degree of Ta incorporation into the silica matrix, (ii) the effect of Ta and Ag loadings
108　and ratio, and (iii) the effect of contact time. By doing so we identify the key parameters that dictate
109　catalyst performance and we propose guidelines for the preparation of more efficient catalysts.
110　Finally, we propose a one-step NHSG method that allows to incorporate both Ta and Ag in the gel.
111　We also show that replacing Ag by Cu leads to a much more active catalyst.
112
113　　　　　　　　$\equiv M-NR_2 + \equiv M-OC(O)R' \rightarrow \equiv M-O-M\equiv + R'C(O)NR_2$　　　　　(1)

114　**2. Results**

115　*2.1. Incorporation of Ta in the silica matrix and impact on catalysis*

116　　　In this section, a catalyst obtained by direct incorporation of Ta into the silica matrix via NHSG
117　followed by Ag impregnation (4TaSi$_{NHSG}$-2Ag) will be described in detail and compared to the
118　corresponding catalyst obtained by the simultaneous impregnation of Ta and Ag (4Ta$_{IMP}$Si-2Ag).
119　First, the textural properties are described, then tantalum dispersion in the materials is studied using
120　ICP, XPS, IR and DRUV studies and finally these properties are confronted with the performance of
121　both samples in the ethanol to butadiene reaction.
122　　　The binary metallosilicate was prepared by the NHSG acetamide route, starting from silicon
123　tetraacetate and pentakis(dimethylamido)tantalum(V), in dichloromethane and in the presence of
124　F127 (see details in the Experimental section). The catalyst is mainly mesoporous, with an evident

125 hysteresis loop in the N$_2$-physisorption isotherms (Figure 1). It shows a specific surface area close to
126 1000 m² g^{-1}, a high pore volume (0.96 cm³ g^{-1}, of which only a small fraction arises from micropores)
127 and an average pore size diameter of 3.9 nm (Table 1). Upon subsequent impregnation of Ag
128 (4TaSi$_{NHSG}$-2Ag) the catalyst tends to lose a fraction of both specific surface area (SSA, −30 %) and
129 pore volume (−32 %) but remains mesoporous and maintains the same average pore size. When the
130 pristine Si$_{NHSG}$ materials prepared by the NHSG acetamide route is simultaneously impregnated with
131 Ta and Ag, a similar drop in SSA and pore volume is observed and the average pore size diameter is
132 also maintained at 4 nm. All in all, both bifunctional catalysts (4Ta$_{IMP}$Si-2Ag and 4TaSi$_{NHSG}$-2Ag)
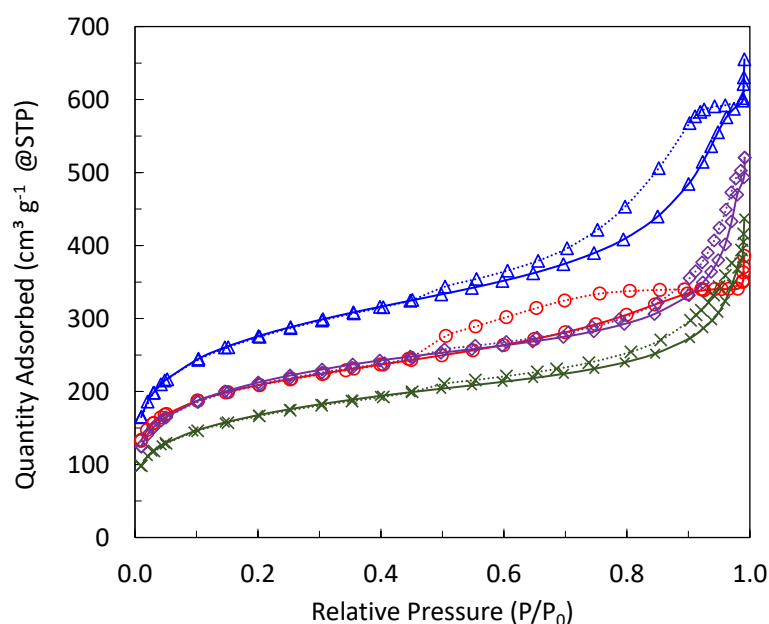133 present a very similar texture.

134

135 **Figure 1.** N$_2$-physisorption isotherms of 4TaSi$_{NHSG}$ (Δ), 4TaSi$_{NHSG}$-2Ag (○), Si$_{NHSG}$ (◊), and 4Ta$_{IMP}$Si-2Ag
136 (×). Adsorption isotherms are plotted as solid lines, desorption isotherms are plotted as dotted lines.

137 **Table 1.** Textural properties (N$_2$-physisorption) and analysis of composition (ICP-OES), surface
138 composition (XPS) and surface acidity (NH$_3$-TPD) for the catalysts prepared with a 4 wt.% Ta loading
139 either by NHSG or dry impregnation (IMP).

Sample	S$_{BET}$ (m² g^{-1})	V$_P$ (cm³ g^{-1})[a]	V$_\mu$ (cm³ g^{-1})[b]	D$_P$ (nm)[c]	% Ta (w/w)[d]	% Ag (w/w)[d]	Surface Si/Ta[e]	Acid sites (mmol g^{-1})[f]
4TaSi$_{NHSG}$[g]	990	0.96	0.17	3.9	4.3	-	65	n.m.
4TaSi$_{NHSG}$-2Ag	690	0.65	0.11	3.8	4.8	1.7	61	3.7 10^{-2}
Si$_{NHSG}$	760	0.76	0.13	4.0	-	-	-	n.m.
4Ta$_{IMP}$Si-2Ag	600	0.59	0.09	4.0	4.1	1.6	34	1.5 10^{-2}

140 [a]Pore volume at P/P$_0$=0.98; [b]Micropore volume at P/P$_0$=0.98; [c]Calculated as 4V$_P$/S$_{BET}$; [d]Determined by
141 ICP; [e]Determined by XPS; [f]Determined by NH$_3$-TPD; [g]if the same formulation is prepared in the
142 absence of F127, a microporous mixed oxide is obtained with V$_P$ = V$_\mu$ = 0.22 cm³ g^{-1}. Thus, for the
143 synthesis with the acetamide route, the use of a texturing agent is mandatory to obtain a
144 mesoporous sample.[26]

145

146 For all catalysts, the experimental composition (ICP-OES) matched closely the nominal values
147 (Table 1), showing that both the non-hydrolytic sol-gel and the impregnation steps were done with a
148 good control over composition.
149 To further assess the active sites dispersion, the molar surface composition was measured by
150 XPS and the Si/Ta ratio was calculated (Table 1). For the catalysts where the tantalum was
151 incorporated through non-hydrolytic sol-gel (4TaSi$_{NHSG}$ and 4TaSi$_{NHSG}$-2Ag), the experimental Si/Ta

152 molar ratio was very close to the theoretical value (60). This suggests a homogeneous dispersion of
153 Ta throughout the metallosilicate materials, without preferential enrichment of the bulk or the
154 surface. When tantalum was incorporated by impregnation (4Ta$_{IMP}$Si-2Ag), the Si/Ta molar ratio
155 reached 34 only, expectedly indicating higher amount of tantalum on the surface.

156   The peak corresponding to the Si 2p orbital always has the expected position at 103.4 eV, which
157 corresponds the expected position for SiO$_2$.[37-38] The binding energies (BE) of the Ta 4f$_{7/2}$ orbital falls
158 around 26.9 eV for 4Ta$_{IMP}$Si-2Ag, very close to the position found for pure Ta$_2$O$_5$.[39-40] On the contrary,
159 for catalysts where tantalum was incorporated by NHSG, a 0.3–0.4 eV shift was consistently observed
160 (Figure 2). This shift can be explained by the difference in electronegativity between Si and Ta:[38, 41]
161 when incorporated into a silica matrix, Ta atoms have a lower electron density and therefore electrons
162 have a higher BE. Similar effect was reported in the case of Ti incorporated in silica,[42] or with V
163 incorporated into titania.[43] Such effect can be taken as an indication of the dispersion of Ta into the
164 silica matrix in the case of NHSG catalysts, as opposed to the case where Ta is brought to the support
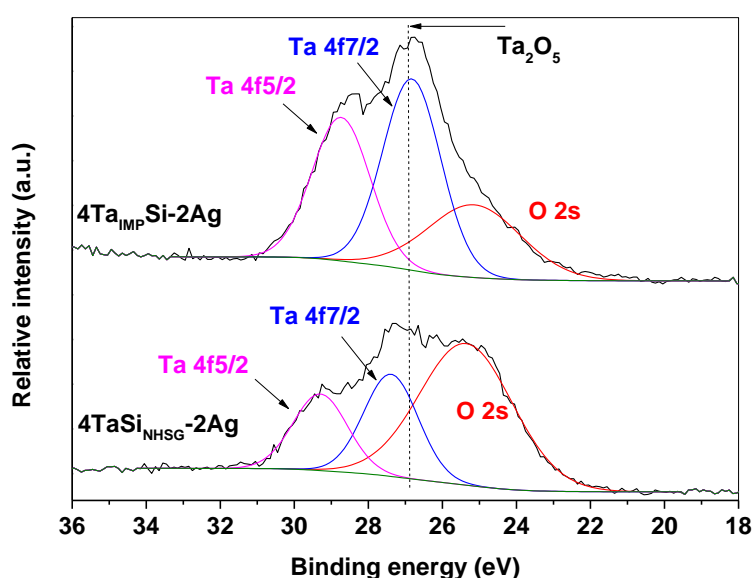165 surface by impregnation.

166

167   **Figure 2.** Binding energy shift of tantalum in XP spectroscopy spectra between Ta impregnated
168   (4Ta$_{IMP}$-2Ag) and Ta one pot (4Ta$_{NHSG}$-2Ag)

169   Tantalum dispersion was also inspected by infrared spectroscopy. The band at 950 cm^{-1}
170 corresponds to the Si–O–Ta bond stretching mode (Figure 3) and the intensity of this band is linked
171 to the amount of Si−O−Ta bonds in the catalyst.[44-45] When Ta is incorporated through NHSG (Figure
172 3), the band at 950 cm^{-1} is better resolved and higher in intensity, as compared to the impregnated
173 catalyst, consistently indicating a greater occurrence of Si–O–Ta bonds in the former case. This
174 difference is another indication of the incorporation of Ta into the silica matrix by NHSG compared
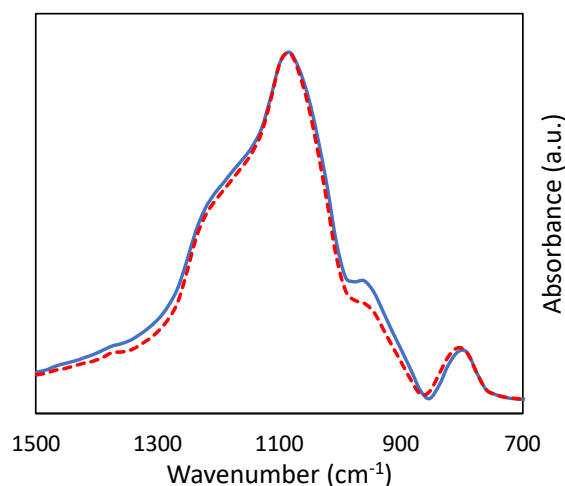175 to the impregnation of Ta that tends to form TaO$_x$ species on the catalyst surface.

Figure 3. FTIR spectra obtained on 4TaSi$_{NHSG}$-2Ag (solid blue line), 4Ta$_{IMP}$Si-2Ag (dotted red line).

In DRUVS (Figure 4), the narrow absorbance band found at around 210 nm for 4TaSi$_{NHSG}$-2Ag can be assigned to mononuclear Ta(V) species, similar to those found in Ta-BEA zeolite where Ta is incorporated in the zeolite structure as single sites.[46] For 4Ta$_{IMP}$Si-2Ag, the broadening of the signal above 220 nm – with a distinct contribution around 260 cm^{-1} – is indicative of the presence of polymeric Ta oxide species.[45, 47] While the presence of such condensed species in 4TaSi$_{NHSG}$-2Ag can not be excluded, their contribution is clearly more important in 4Ta$_{IMP}$Si-2Ag. Thus, DRUVS confirms that NHSG allows to form relatively high fraction of isolated Ta(V) sites incorporated in silica, while impregnation results in the formation of polymeric TaO$_x$ species.
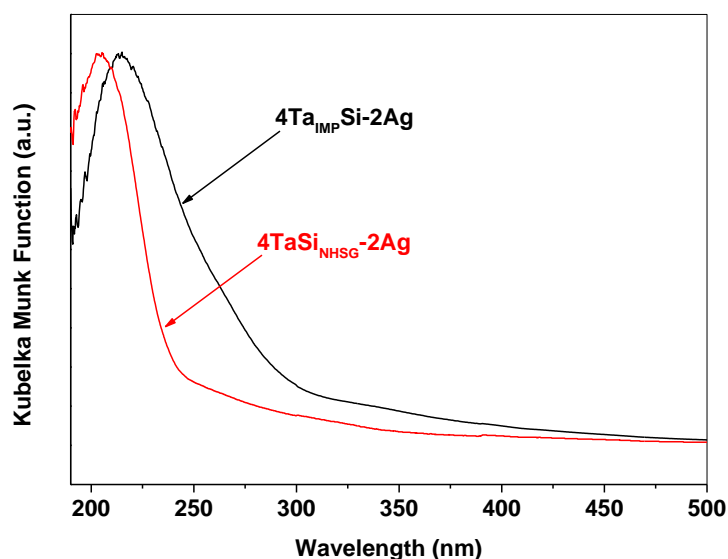

Figure 4. DRUV spectra obtained for 4TaSi$_{NHSG}$-2Ag and 4Ta$_{IMP}$Si-2Ag

The quality of the dispersion of Ta has a marked impact on the catalysts acidity. It has been reported that – unlike tantalum oxide – Ta incorporated as single sites within the crystalline structure of a zeolites displays high acidity.[22, 45] Similarly, it can be expected that Ta incorporated as single sites in an amorphous silica matrix can be expected to exhibit high acidity. Indeed, despite having a much lower Ta surface concentration (XPS), 4TaSi$_{NHSG}$-2Ag shows a number of surface acid sites 2.5 times higher as compared to 4Ta$_{IMP}$Si-2Ag (Table 1). This corroborates again the formation of a true metallosilicate via NHSG, featuring a high dispersion of Ta.

195   In the ethanol-to-butadiene reaction, both catalysts exhibited a similar butadiene yield: 10% and
196 12% respectively for 4TaSi$_{NHSG}$-2Ag and 4Ta$_{IMP}$Si-2Ag (Table 2). In fact, the impregnated catalyst was
197 much less active but much more selective towards butadiene. Interestingly, the ethylene yield was
198 much higher for the catalyst prepared by the direct incorporation of Ta via NHSG. Ethylene results
199 from the direct dehydration of ethanol and is catalyzed by acid sites.[48-50] As demonstrated above,
200 when Ta is incorporated through NHSG, a high Ta dispersion is obtained, resulting in the formation
201 of a much more acidic catalyst, owing to the presence of a larger fraction of Si–O–Ta bonds (isolated
202 Ta sites). Thus, the modest butadiene yield obtained with 4TaSi$_{NHSG}$-2Ag can be attributed to an
203 excessive dehydration activity: a large proportion of the ethanol feed is rapidly converted to ethylene
204 instead of forming acetaldehyde or reacting with crotonaldehyde to continue the cascade towards
205 butadiene.

206
207

208 **Table 2.** Catalytic conversion of ethanol, yield and selectivity for butadiene and by-products;
209 Reaction conditions: T=355 °C, WHSV=1.10h^{-1}

Catalyst	Ethanol conversion (%)	Butadiene (%)		Acetaldehyde (%)		Ethylene (%)		Diethylether (%)		Others (%)	
		Yield	Sel	Yield	Sel	Yield	Sel	Yield	Sel	Yield	Sel
4Ta$_{IMP}$Si-2Ag	53.7	12.1	22.5	13.3	24.8	7.7	14.3	10.3	19.2	10.3	19.2
4TaSi$_{NHSG}$-2Ag	78.1	10.4	13.3	17.0	21.8	28.9	37.0	8.1	10.4	13.8	17.7
4TaSi$_{NHSG}$-5Ag	90.4	15.4	17.0	17.1	18.9	31.5	34.8	5.3	5.9	21.1	23.3
2TaSi$_{NHSG}$-2Ag	64.8	4.6	7.1	17.3	26.7	23.6	36.4	7.2	11.1	12.1	18.7
2TaSi5Ag$_{NHSG}$	65.2	8.9	13.7	19.9	30.5	22.2	34.0	4.9	7.5	9.5	14.6
2TaSi5Cu$_{NHSG}$	75.3	23.3	30.9	29.8	39.6	1.4	1.9	0.8	1.1	20.0	26.6

210

211 *2.2. Influence of tantalum and silver loading on butadiene yield*

212   In a search for a better balance between the acid (dehydration) and the redox (dehydrogenation)
213 functions of the catalyst prepared by NHSG, the silver and tantalum loadings have been modified.
214 When keeping the 4% Ta incorporated by NHSG but increasing the silver loading to 5%
215 (4TaSi$_{NHSG}$-5Ag), both the ethanol conversion and the butadiene yield increase. Ethylene and
216 diethylether yields remain at the same level as well, suggesting that the dehydration power of the
217 catalyst is similar, regardless of the silver loading. In fact, surface acid site density determined by
218 NH$_3$-TPD was found to be the same as for 4TaSi$_{NHSG}$-2Ag (3.7 10^{-2} mmol g^{-1}). The production of
219 acetaldehyde remains fairly constant suggesting that a higher proportion of the acetaldehyde that is
220 obtained through dehydrogenation further undergoes self-condensation that allows proceeded
221 towards butadiene formation.
222   When keeping a 2 wt.% silver loading but decreasing the Ta loading to 2 wt.% to mitigate the
223 dehydration activity (2TaSi$_{NHSG}$-2Ag), the ethanol conversion decreases and the butadiene yield drops
224 dramatically. In fact, the selectivity to dehydration products (ethene and diethyl ether) remains fairly
225 constant, but the catalyst is simply less active probably because there is a lower density of strong
226 surface acid sites, which accounts for a lower conversion and lower yields in dehydration products.
227 Dehydrogenation towards acetaldehyde is still produced in appreciable amounts; yet its further
228 conversion to butadiene remains modest, possibly because the next steps of the mechanism also
229 require acid sites in substantial amounts.
230   While the best performance was obtained with the 4TaSi$_{NHSG}$-5Ag, we suggest that further
231 research is required to determine the optimal Ta and Ag loadings in these bifunctional catalysts, so
232 as to guide the intricate reaction scheme towards the production of butadiene. Instead of tuning the
233 catalyst composition, playing on the operational parameters is also a relevant approach to enhance
234 the butadiene yields. Figure 5 shows how the butadiene and acetaldehyde yields are affected by space

velocity. When the WHSV is decreased, the yield to acetaldehyde drops and the yield to butadiene is boosted. By decreasing the WHSV, the contact time between the reagents and the active sites is increased. Consequently, a higher fraction of the acetaldehyde that is produced through dehydrogenation has the opportunity to undergo self-condensation, leading to acetaldol which is further converted to crotonaldehyde and then butadiene. This increase in yield, however, comes at the cost of a lower butadiene productivity.
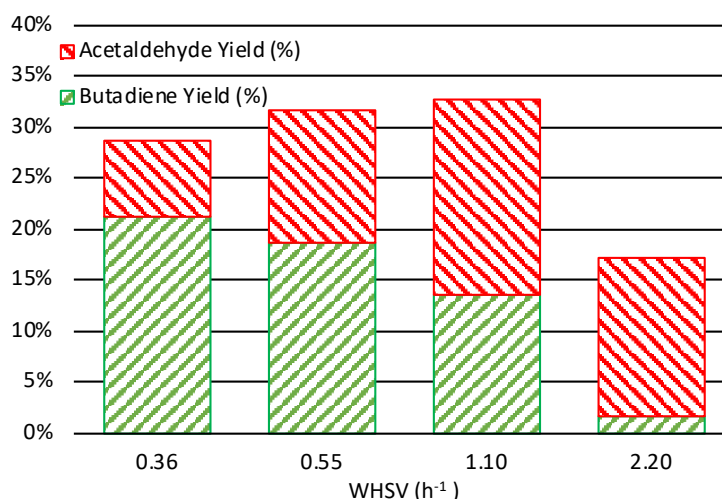

Figure 5. Butadiene and acetaldehyde yields as a function of the contact time for 4TaSi$_{NHSG}$-5Ag at 355 °C.

2.3. One-pot NHSG preparation of Ag-TaSiO$_2$ bifunctional catalyst

To further leverage on the versatility of the NHSG process, a one-step preparation of bifunctional catalysts was developed. The idea is to incorporate Ag directly in the NHSG protocol, thereby circumventing the need for a subsequent impregnation step. In this case, a precise amount of (bis)dodecylamine-silver – corresponding to a 5 wt.% nominal loading – was added in the precursor solution right before placing the autoclave in the oven for polycondensation. Also, the solvent was changed to toluene (instead of dichloromethane that was inducing the formation of AgCl) and Brij58 was used as the templating agent (instead of F127 which has a relatively low solubility in toluene). The catalyst prepared via this one-pot approach (2TaSi5Ag$_{NHSG}$) also exhibited a favorable texture: S$_{BET}$ = 710 m^2 g^{-1}, V$_P$ = 0.89 cm^3 g^{-1}, D$_P$ = 5.0 nm. Ag nanoparticles could be observed in TEM, dispersed throughout the highly porous Ta-SiO$_2$ matrix, with a relatively large size distribution (1-30 nm) (Figure 6). This catalyst was also able to catalyze the dehydration and dehydrogenation reactions, yet the butadiene yield remained modest as compared to the best catalysts discussed previously (prepared in two steps).
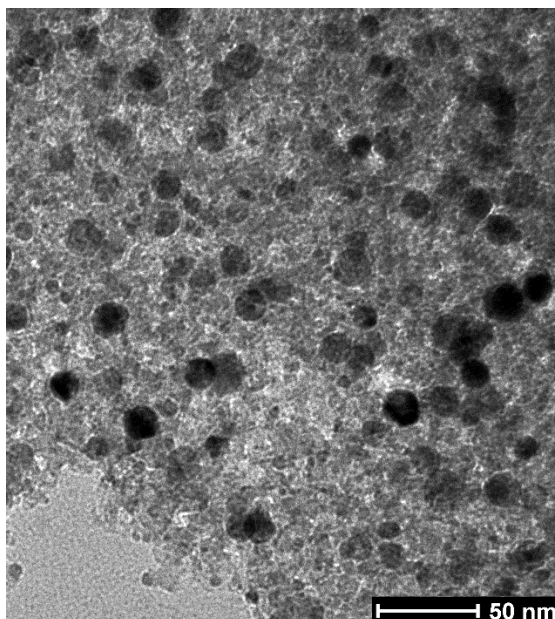
Figure 6. TEM micrograph of the 2TaSi5Ag$_{NHSG}$ catalyst

2.4. Copper as an effective alternative to silver

The same strategy was adopted to prepare a 2TaSi5Cu$_{NHSG}$ catalyst, using copper(II) acetylacetonate as a source of Cu. The texture was again very similar (S_{BET} = 640 m^2 g^{-1}, V_P = 0.60 cm^3 g^{-1}, D_P = 3.8 nm). The butadiene yield, however, was almost three times higher as compared to the corresponding Ag-based catalyst, reaching 23 % (**Table 2**). The higher performance of Cu-promoted catalysts as compared to Ag-promoted catalysts was already reported by Kyriienko et al.[16] and attributed to a higher dehydrogenation activity. It was also suggested that the metal doping can modify the acid-base properties of the support, thereby affecting the dehydration activity as well. Indeed, with the Cu-based catalysts, we observe a very low yield in dehydration products. This suggests that a better balance was found, with an efficient dehydrogenation activity and a moderate dehydration activity. In the next steps of this research, we plan to further study the impact of the Ta and Cu loadings, in a search for higher butadiene yields.

3. Conclusion

Non-hydrolytic sol-gel (NHSG) and more specifically the acetamide elimination route is shown to be an effective method to incorporate tantalum in a silica matrix, resulting in a highly homogeneous acidic mixed oxide. With the addition of a templating agent (Pluronic F127), the catalysts display a mesoporous texture with relatively large pore volumes and high specific surface area. Importantly, several characterization tools, allowed us to demonstrate that Ta is mainly incorporated as highly dispersed species into the silica. As a result, even if the surface concentration is lower than in a catalyst prepared by simple impregnation, the density of acid sites is significantly higher in the NHSG-made catalyst. Upon promotion with Ag, the catalyst becomes active in the ethanol to butadiene reaction, even if butadiene yields remain modest. In fact, the selectivity toward ethylene is high, which indicates that the catalyst dehydration power is too high as compared to its dehydrogenation power. Tuning down the acidity by decreasing the Ta loading from 4 to 2 wt.% does not allow reaching higher performance, presumably because acid sites are also needed for the further steps of the reaction mechanism. Increasing the Ag loading results in a higher butadiene yield, showing that the key for further improvement is probably to enhance the dehydrogenation activity. The contact time is also shown to have a great impact on the butadiene yields. Interestingly, we show that bifunctional catalysts can be prepared in one step using NHSG. Ag/Ta-SiO$_2$ and Cu/Ta-SiO$_2$ catalysts were prepared in this way and we show that Cu doping results in much higher butadiene yield as compared to the corresponding Ag-doped catalysts.

4. Experimental

4.1. Catalyst preparation

General. NHSG processes were performed under Ar atmosphere or high vacuum by using the Schlenk line and a dry box with H_2O and O_2 levels below 1 ppm. CH_2Cl_2 (Carl Roth, ≥ 99.8 %) was dried with P_4O_{10}. Toluene (Carl Roth, ≥ 99.5 %) was dried over Na metal. All solvents were distilled and stored in a glovebox under molecular sieves. Silicon tetraacetate, pentakis(dimethylamido)tantalum(V) and silver bis(dodecylamine) nitrate were prepared according to literature[51-53] and stored in a glovebox. Silicon tetrachloride (Acros Organics, 99.8 %), ethanol absolute (AnalaR NORMAPUR, 99.95 %), silver nitrate (VWR, 99.9 %), dodecylamine (VWR, ≥ 97.0 %), copper(II) acetylacetonate (TCI, 97 %), tantalum(V) ethoxide (ABCR, 99.99 %) and acetonitrile (VWR, isocratic grade) were used as received. Pluronic F127 and Brij 58 (Sigma-Aldrich) were dried under vacuum at 100 °C overnight and stored in a glovebox.

Xerogel synthesis. For the synthesis of $Ta\text{-}SiO_2$ binary oxides, silicon tetraacetate and Pluronic F127 were loaded in a Teflon autoclave in a glovebox and dissolved in 40 cm^3 of dichloromethane (for the exact quantities involved in each preparation, see supplementary materials, Table S1). In a separate vial pentakis(dimethylamido)tantalum(V) was dissolved in dichloromethane. This solution was then added to the solution of $Si(OAc)_4$ and Pluronic F127 while stirring. The autoclave was sealed and kept in an oven at 160 °C for 72 hrs for the gelation. Afterwards, the autoclave was cooled down and put back into the glovebox, opened and the gel was transferred into a Schlenk flask. The gel was dried under vacuum at 60 °C overnight to remove solvent and volatile condensation products (dimethylacetamide and acetic acid anhydride). Finally, the resulting powder was calcined at 500 °C (flowing air, 5 °C min^{-1}, 5 hrs) to obtain a white catalyst. Samples are denoted XTaSi$_{NHSG}$ where "X" is the nominal Ta wt.% in the metallosilicate (either 2 or 4 wt.%). A silica sample was synthesized as a reference pristine support, using the same protocol but with only a very small amount of Ta (small amount of Lewis acid is necessary to induce the polycondensation reactions). The sample is denoted Si$_{NHSG}$ and actually contains a nominal loading of 0.1 wt.% Ta.

Dry impregnation. After calcination, TaSi$_{NHSG}$ materials were impregnated with 2 or 5 % silver. The appropriate amount of silver nitrate was weighted (see Table S2) and dissolved in a volume of water corresponding to the pore volume of the catalyst to impregnate. The solution was put in an ultrasonic bath for 15 minutes to allow the dissolution of silver nitrate and then added to 1 g of TaSi$_{NHSG}$ catalyst. The mixture was stirred until a thick paste was obtained. The paste was put to rest for 1 hour at RT and then dried in an oven at 100 °C to evaporate the water. Finally, the powder was calcined again at 500 °C (flowing air, 5 °C min^{-1}, 5 hrs). For comparison, a sample was prepared by impregnation of both Ta and Ag on the Si$_{NHSG}$ support (4Ta$_{IMP}$-2Ag). 47.5 mg of $Ta(OEt)_5$ and 16.7 mg of $AgNO_3$ were dissolved in ethanol and added to 0.5 g of Si$_{NHSG}$ using the same impregnation protocol.

4.2. Characterization

Textural properties (surface area, pore volume, pore size) were determined by nitrogen physisorption at 77.4 K on a Tristar 3000 instrument from Micromeritics, USA. Prior to measurement, samples were degassed at 150 °C for 8 hrs minimum. The specific surface area was determined by the BET method with at least five data points with relative pressure between 0.05 and 0.3. Silicon, tantalum and silver content were determined on an ICP optical emission spectrometer iCAP 6500 Duo from Thermo, UK equipped with a solid-state generator with a frequency of 27.12 MHz and a maximum power input of 1350 W. X-ray photoelectron spectroscopy measurements were carried out on a SSI X probe spectrometer (model SSI 100, Surface Science Laboratories, Mountain View, CA) equipped with a monochromatized Al-Kα radiation (1486 eV). The catalyst powders previously pressed in small stainless troughs of 4 mm diameter, were placed on an insulating home-made ceramic carousel. The pressure in the analysis chamber was set at around 10^{-6} Pa. The analyzed area was approximately 1.4 mm^2 and the pass energy was set at 150 eV. The C1s peak of carbon has been fixed to 284.8 eV to set the binding energy scale.[54] Data treatment was performed with the CasaXPS

343 program (Casa Software Ltd, UK) and spectra were decomposed with the least squares fitting routine
344 provided by the software with a Gaussian/Lorentzian (85/15) product function and after baseline
345 subtraction. Temperature programmed desorption of ammonia (NH_3-TPD) was performed on a
346 Hiden CATLAB-PCS microreactor connected to a mass spectrometer equipped with a quadrupole
347 separator. Samples (400–800 μm particle size) were first dehydrated at 300 °C (10 °C min^{-1}) for 1 hr
348 under Ar (40 ml min^{-1}). Ammonia adsorption took place at 150 °C for 40 minutes (20 ml min^{-1} of Ar,
349 5 %vol NH_3) before a 80 minutes purge under Ar (40 ml min^{-1}). The temperature was then increased
350 to 600 °C (10 °C min^{-1}) to desorb ammonia. FTIR spectra (4000–400 cm^{-1}) were recorded on a Bruker
351 Equinox 55 spectrometer (transmission mode, through KBr pellets). DRUV spectra (150–500 nm)
352 were recorded on a Shimadzu UV-3600Plus.

353 *4.3. Ethanol to butadiene reaction*

354 Calcined catalysts (0.192 g, pressed and sieved in the 0.20–0.40 mm particle size range) were
355 diluted with glass beads (0.5–1 mm) in order to keep the volume of the catalyst bed constant. The rest
356 of the tubular reactor (stainless steel, 0.6 cm internal diameter) was filled with silica beads. Before
357 reaction, the catalyst was pretreated in situ by feeding hydrogen (30 vol.% H_2 in N_2) for 1 hr at 355 °C
358 (silver/copper reduction). Catalytic testing was carried out by feeding 0.212 g h^{-1} of ethanol absolute
359 (fed with a NE-300 syringe pump) and 40 cm^3 min^{-1} of nitrogen (4.4 mol.% of ethanol in N_2), WHSV
360 = 1.1 h^{-1}. The tests were carried out at atmospheric pressure and at 355°C. After a stabilization of 10
361 minutes at the set temperature, effluent gas were analyzed on a VARIAN 3800 Gas Chromatograph
362 (5 injections at each temperature) equipped with a flame ionization detector (FID) and a Restek Rt-
363 U-Bond column (30 m long, internal diameter of 0.32 mm, film thickness of 10 μm).
364

370

371 **References**

372 1. Cespi, D.; Passarini, F.; Vassura, I.; Cavani, F., Butadiene from biomass, a life cycle perspective to
373 address sustainability in the chemical industry. *Green Chem.* **2016,** *18* (6), 1625-1638.

374 2. Shylesh, S.; Gokhale, A. A.; Scown, C. D.; Kim, D.; Ho, C. R.; Bell, A. T., From Sugars to Wheels: The
375 Conversion of Ethanol to 1,3-Butadiene over Metal-Promoted Magnesia-Silicate Catalysts. *ChemSusChem* **2016,** *9*
376 (12), 1462-1472.

377 3. Pomalaza, G.; Capron, M.; Ordomsky, V.; Dumeignil, F.; Pomalaza, G.; Capron, M.; Ordomsky, V.;
378 Dumeignil, F., Recent Breakthroughs in the Conversion of Ethanol to Butadiene. *Catalysts* **2016,** *6* (12), 203.

379 4. White, W. C., Butadiene production process overview. *Chem. Biol. Interact.* **2007,** *166* (1-3), 10-14.

380 5. Ren, T.; Patel, M.; Blok, K., Olefins from conventional and heavy feedstocks: Energy use in steam
381 cracking and alternative processes. *Energy* **2006,** *31* (4), 425-451.

382 6. Chaudhary, L.; Pradhan, P.; Soni, N.; Singh, P.; Tiwari, A., Algae as a feedstock for bioethanol
383 production: new entrance in biofuel world. *International Journal of ChemTech Research* **2014,** *6* (2), 1381-1389.

384 7. Muktham, R.; K. Bhargava, S.; Bankupalli, S.; S. Ball, A., A Review on 1st and 2nd Generation Bioethanol
385 Production-Recent Progress. *Journal of Sustainable Bioenergy Systems* **2016,** *06* (03), 72-92.

386 8. Gérardy, R.; Morodo, R.; Estager, J.; Luis, P.; Debecker, D. P.; Monbaliu, J.-C. M., Sustaining the
387 Transition from a petrobased to a Biobased Chemical Industry with Flow Chemistry. *Topics in Current Chemistry*
388 **2019,** *377* (1), 1.

389   9.   Gallezot, P., Conversion of biomass to selected chemical products. *Chem. Soc. Rev.* **2012,** *41* (4), 1538-
390   1558.

391   10.   Dumeignil, F.; Capron, M.; Katryniok, B.; Wojcieszak, R.; Löfberg, A.; Girardon, J.-S.; Desset, S.; Araque-
392   Marin, M.; Jalowiecki-Duhamel, L.; Paul, S., Biomass-derived platform molecules upgrading through catalytic
393   processes: yielding chemicals and fuels. *Journal of the Japan Petroleum Institute* **2015,** *58* (5), 257-273.

394   11.   Kim, T.-W.; Kim, J.-W.; Kim, S.-Y.; Chae, H.-J.; Kim, J.-R.; Jeong, S.-Y.; Kim, C.-U., Butadiene production
395   from bioethanol and acetaldehyde over tantalum oxide-supported spherical silica catalysts for circulating
396   fluidized bed. *Chemical Engineering Journal* **2015,** *278*, 217-223.

397   12.   Sun, J.; Wang, Y., Recent Advances in Catalytic Conversion of Ethanol to Chemicals. *ACS Catal.* **2014,** *4*
398   (4), 1078-1090.

399   13.   Makshina, E. V.; Dusselier, M.; Janssens, W.; Degrève, J.; Jacobs, P. A.; Sels, B. F., Review of old
400   chemistry and new catalytic advances in the on-purpose synthesis of butadiene. *Chem. Soc. Rev.* **2014,** *43* (22),
401   7917-7953.

402   14.   Talalay, A.; Talalay, L., S. K.—The Russian Synthetic Rubber from Alcohol. A Survey of the Chemistry
403   and Technology of the Lebedev Process for Producing Sodium-Butadiene Polymers. *Rubber Chemistry and*
404   *Technology* **1942,** *15* (3), 403-429.

405   15.   Corson, B. B.; Jones, H. E.; Welling, C. E.; Hinckley, J. A.; Stahly, E. E., Butadiene from Ethyl Alcohol.
406   Catalysis in the One-and Two-Stop Processes. *Ind. Eng. Chem.* **1950,** *42* (2), 359-373.

407   16.   Kyriienko, P. I.; Larina, O. V.; Soloviev, S. O.; Orlyk, S. M.; Calers, C.; Dzwigaj, S., Ethanol Conversion
408   into 1,3-Butadiene by the Lebedev Method over MTaSiBEA Zeolites (M = Ag, Cu, Zn). *ACS Sus. Chem. Eng.* **2017,**
409   *5* (3), 2075-2083.

410   17.   Angelici, C.; Weckhuysen, B. M.; Bruijnincx, P. C. A., Chemocatalytic Conversion of Ethanol into
411   Butadiene and Other Bulk Chemicals. *ChemSusChem* **2013,** *6* (9), 1595-1614.

412   18.   Müller, P.; Burt, S. P.; Love, A. M.; McDermott, W. P.; Wolf, P.; Hermans, I., Mechanistic Study on the
413   Lewis Acid Catalyzed Synthesis of 1,3-Butadiene over Ta-BEA Using Modulated Operando DRIFTS-MS. *ACS*
414   *Catal.* **2016,** *6* (10), 6823-6832.

415   19.   Sushkevich, V. L.; Ivanova, I. I.; Ordomsky, V. V.; Taarning, E., Design of a Metal-Promoted Oxide
416   Catalyst for the Selective Synthesis of Butadiene from Ethanol. *ChemSusChem* **2014,** *7* (9), 2527-2536.

417   20.   Sushkevich, V. L.; Ivanova, I. I.; Taarning, E., Mechanistic Study of Ethanol Dehydrogenation over
418   Silica-Supported Silver. *ChemCatChem* **2013,** *5* (8), 2367-2373.

419   21.   Sushkevich, V. L.; Ivanova, I. I.; Taarning, E., Ethanol conversion into butadiene over Zr-containing
420   molecular sieves doped with silver. *Green Chem.* **2015,** *17* (4), 2552-2559.

421   22.   Kyriienko, P. I.; Larina, O. V.; Soloviev, S. O.; Orlyk, S. M.; Dzwigaj, S., High selectivity of TaSiBEA
422   zeolite catalysts in 1,3-butadiene production from ethanol and acetaldehyde mixture. *Catalysis Communications*
423   **2016,** *77*, 123-126.

424   23.   Debecker, D. P., Innovative Sol-Gel Routes for the Bottom-Up Preparation of Heterogeneous Catalysts.
425   *The Chemical Record* **2018,** *18* (7-8), 662-675.

426   24.   Livage, J., Sol–gel synthesis of heterogeneous catalysts from aqueous solutions. *Catalysis Today* **1998,** *41*
427   (1), 3-19.

428   25.   Debecker, D. P.; Mutin, P. H., Non-hydrolytic sol-gel routes to heterogeneous catalysts. *Chem Soc Rev*
429   **2012,** *41* (9), 3624-50.

430   26.   Skoda, D.; Styskalik, A.; Moravec, Z.; Bezdicka, P.; Babiak, M.; Klementova, M.; E. Barnes, C.; Pinkas,
431   J., Novel non-hydrolytic templated sol–gel synthesis of mesoporous aluminosilicates and their use as aminolysis
432   catalysts. *RSC Advances* **2016,** *6* (29), 24273-24284.

433 27. Skoda, D.; Styskalik, A.; Moravec, Z.; Bezdicka, P.; Pinkas, J., Templated non-hydrolytic synthesis of

434 mesoporous zirconium silicates and their catalytic properties. *J Mater Sci* **2015,** *50* (9), 3371-3382.

435 28. Styskalik, A.; Skoda, D.; Barnes, C.; Pinkas, J.; Styskalik, A.; Skoda, D.; Barnes, C. E.; Pinkas, J., The

436 Power of Non-Hydrolytic Sol-Gel Chemistry: A Review. *Catalysts* **2017,** *7* (6), 168.

437 29. Styskalik, A.; Skoda, D.; Pinkas, J.; Mathur, S., Non-hydrolytic synthesis of titanosilicate xerogels by

438 acetamide elimination and their use as epoxidation catalysts. *J Sol-Gel Sci Technol* **2012,** *63* (3), 463-472.

439 30. Debecker, D. P.; Hulea, V.; Mutin, P. H., Mesoporous mixed oxide catalysts via non-hydrolytic sol–gel:

440 A review. *Applied Catalysis A: General* **2013,** *451*, 192-206.

441 31. Bouchmella, K.; Stoyanova, M.; Rodemerck, U.; Debecker, D. P.; Hubert Mutin, P., Avoiding rhenium

442 loss in non-hydrolytic synthesis of highly active Re–Si–Al olefin metathesis catalysts. *Catal. Commun.* **2015,** *58*,

443 183-186.

444 32. Maksasithorn, S.; Praserthdam, P.; Suriye, K.; Devillers, M.; Debecker, D. P., WO3-based catalysts

445 prepared by non-hydrolytic sol-gel for the production of propene by cross-metathesis of ethene and 2-butene.

446 *Appl. Catal. A* **2014,** *488*, 200-207.

447 33. Smeets, V.; Ben Mustapha, L.; Schnee, J.; Gaigneaux, E. M.; Debecker, D. P., Mesoporous SiO2-TiO2

448 epoxidation catalysts: Tuning surface polarity to improve performance in the presence of water. *Molecular*

449 *Catalysis* **2018,** *452*, 123-128.

450 34. Lafond, V.; Mutin, P.; Vioux, A., Non-hydrolytic sol–gel routes based on alkyl halide elimination:

451 Toward better mixed oxide catalysts and new supports: Application to the preparation of a SiO2–TiO2

452 epoxidation catalyst. *Journal of Molecular Catalysis A: Chemical* **2002,** *182*, 81-88.

453 35. Cojocariu, A. M.; Mutin, P. H.; Dumitriu, E.; Fajula, F.; Vioux, A.; Hulea, V., Non-hydrolytic synthesis

454 of mesoporous silica–titania catalysts for the mild oxidation of sulfur compounds with hydrogen peroxide. *Chem.*

455 *Commun.* **2008,** (42), 5357-5359.

456 36. Hamden, Z.; Bouattour, S.; Ferraria, A.; Ferreira, D.; Ferreira, L. V.; Do Rego, A. B.; Boufi, S., In situ

457 generation of TiO2 nanoparticles using chitosan as a template and their photocatalytic activity. *Journal of*

458 *Photochemistry and Photobiology A: Chemistry* **2016,** *321*, 211-222.

459 37. Zatsepin, A.; Zatsepin, D.; Boukhvalov, D.; Kuznetsova, Y. A.; Gavrilov, N.; Shur, V. Y.; Esin, A., Local

460 atomic configurations, energy structure, and optical properties of implantation defects in Gd-doped silica glass:

461 An XPS, PL, and DFT study. *Journal of Alloys and Compounds* **2019,** *796*, 77-85.

462 38. Jacquemin, M.; Genet, M. J.; Gaigneaux, E. M.; Debecker, D. P., Calibration of the X-Ray Photoelectron

463 Spectroscopy Binding Energy Scale for the Characterization of Heterogeneous Catalysts: Is Everything Really

464 under Control? *ChemPhysChem* **2013,** *14* (15), 3618-3626.

465 39. Simpson, R.; White, R. G.; Watts, J. F.; Baker, M. A., XPS investigation of monatomic and cluster argon

466 ion sputtering of tantalum pentoxide. *Applied Surface Science* **2017,** *405*, 79-87.

467 40. Arnould, C.; Volcke, C.; Lamarque, C.; Thiry, P. A.; Delhalle, J.; Mekhalif, Z., Titanium modified with

468 layer-by-layer sol–gel tantalum oxide and an organodiphosphonic acid: A coating for hydroxyapatite growth.

469 *Journal of colloid and interface science* **2009,** *336* (2), 497-503.

470 41. Greczynski, G.; Hultman, L., X-ray photoelectron spectroscopy: Towards reliable binding energy

471 referencing. *Prog. Mater Sci.* **2019**, 100591.

472 42. Hasegawa, Y.; Ayame, A., Investigation of oxidation states of titanium in titanium silicalite-1 by X-ray

473 photoelectron spectroscopy. *Catalysis today* **2001,** *71* (1-2), 177-187.

474 43. Debecker, D. P.; Bouchmella, K.; Delaigle, R.; Eloy, P.; Poleunis, C.; Bertrand, P.; Gaigneaux, E. M.;

475 Mutin, P. H., One-step non-hydrolytic sol–gel preparation of efficient V2O5-TiO2 catalysts for VOC total

476 oxidation. *Appl. Catal. B* **2010,** *94* (1–2), 38-45.

477   44.   Blanc, D.; Zhang, W.; Massard, C.; Mugnier, J., Synthesis and characterisation of tantalum-
478   incorporating silica hybrid sol–gel thin films for optical applications. *Optical Materials* **2006,** *28* (4), 331-335.

479   45.   Ko, Y. S.; Ahn, W. S., Synthesis and characterization of tantalum silicalite molecular sieves with MFI
480   structure. *Microporous and mesoporous materials* **1999,** *30* (2-3), 283-291.

481   46.   Ruddy, D. A.; Tilley, T. D., Kinetics and mechanism of olefin epoxidation with aqueous H2O2 and a
482   highly selective surface-modified TaSBA15 heterogeneous catalyst. *Journal of the American Chemical Society* **2008,**
483   *130* (33), 11088-11096.

484   47.   Dzwigaj, S.; Millot, Y.; Che, M., Ta (V)-single site BEA zeolite by two-step postsynthesis method:
485   preparation and characterization. *Catal Lett* **2010,** *135* (3-4), 169-174.

486   48.   Styskalik, A.; Kordoghli, I.; Poleunis, C.; Delcorte, A.; Aprile, C.; Fusaro, L.; Debecker, D. P., Highly
487   Porous Hybrid Metallosilicate Materials Prepared by Non-Hydrolytic Sol-Gel: Hydrothermal Stability and
488   Catalytic Properties in Ethanol Dehydration. *ChemRxiv - preprint* **2019**, DOI:10.26434/chemrxiv.9114413.v1.

489   49.   Debecker, D. P.; Boissiere, C.; Laurent, G.; Huet, S.; Eliaers, P.; Sanchez, C.; Backov, R., First acidic
490   macro-mesocellular aluminosilicate monolithic foams "SiAl(HIPE)" and their catalytic properties. *Chem.*
491   *Commun.* **2015,** *51* (74), 14018-14021.

492   50.   Phung, T. K.; Busca, G., Ethanol dehydration on silica-aluminas: Active sites and ethylene/diethyl ether
493   selectivities. *Catal. Commun.* **2015,** *68*, 110-115.

494   51.   Balthis, J.; Rochow, E.; White, D., Silicon Tetraacetate. *Inorganic Syntheses* **1953,** *4*, 45-47.

495   52.   Bradley, D. C.; Thomas, I. M., METALLO-ORGANIC COMPOUNDS CONTAINING METAL–
496   NITROGEN BONDS: PART III. DIALKYLAMINO COMPOUNDS OF TANTALUM. *Canadian Journal of*
497   *Chemistry* **1962,** *40* (7), 1355-1360.

498   53.   Wakuda, D.; Hatamura, M.; Suganuma, K., Novel method for room temperature sintering of Ag
499   nanoparticle paste in air. *Chemical Physics Letters* **2007,** *441* (4-6), 305-308.

500   54.   Jacquemin, M.; Genet, M. J.; Gaigneaux, E. M.; Debecker, D. P., Calibration of the X-Ray Photoelectron
501   Spectroscopy Binding Energy Scale for the Characterization of Heterogeneous Catalysts: Is Everything Really
502   under Control? *ChemPhysChem* **2013,** *14* (15), 3618-3626.

503

504

505